

A Search for Axionic Dark Matter Using the Magnetar PSR J1745–2900

Jeremy Darling

*Center for Astrophysics and Space Astronomy
Department of Astrophysical and Planetary Sciences
University of Colorado, 389 UCB
Boulder, CO 80309-0389, USA**

(Dated: August 19, 2020)

We report on a search for dark matter axion conversion photons from the magnetosphere of the Galactic Center magnetar PSR J1745–2900 using spectra obtained from the Karl G. Jansky Very Large Array.^a No significant spectral features are detected. Using a hybrid model for PSR J1745–2900 and canonical assumptions about the dark matter density profile, we exclude axion models with axion-photon coupling $g_{a\gamma\gamma} > 6\text{--}34 \times 10^{-12} \text{ GeV}^{-1}$ with 95% confidence over the mass ranges 4.2–8.4, 18.6–26.9, 33.0–41.4, 53.7–62.1, and 126.0–159.3 μeV . If there is a dark matter cusp, the limits reduce to $g_{a\gamma\gamma} > 6\text{--}34 \times 10^{-14} \text{ GeV}^{-1}$, which overlap some axion models for the observed mass ranges $> 33 \mu\text{eV}$. These limits may be improved by modeling the stimulated emission that can boost the axion-photon conversion process.

INTRODUCTION

The axion is a spin zero chargeless massive particle introduced to address the strong CP (charge-parity) problem in quantum chromodynamics (QCD; [1–3]). If they exist, QCD axions are likely to be produced in the early universe, are a promising cold dark matter candidate [4–6], and may explain the cosmic matter-antimatter asymmetry [7].

Axions couple to QCD and electromagnetism. The electromagnetic coupling $\mathcal{L}_{a\gamma\gamma} = -(1/4)g_{a\gamma\gamma}a F_{\mu\nu}\tilde{F}^{\mu\nu} = g_{a\gamma\gamma}a \mathbf{E} \cdot \mathbf{B}$ suggests that axion-photon conversion can occur in the presence of magnetic fields, but the axion-photon coupling is weak ($g_{a\gamma\gamma} \sim 10^{-16} \text{ GeV}^{-1}$ for axion mass $m_a = 1 \mu\text{eV}$) [8–12]. The relationship between $g_{a\gamma\gamma}$ and m_a is linear, but the mass is not constrained; axion searches must span decades in m_a .

Recent axion searches include CAST, which searched for Solar axions [13, 14], and haloscopes such as ADMX and HAYSTAC that use narrow-band resonant cavities to detect dark matter axions [15–18]. There are also natural settings where telescopes may conduct sensitive and wide-band QCD axion searches [19–27].

The Galactic Center magnetar PSR J1745–2900 offers an ideal setting for an axion conversion line search: it has a strong magnetic field ($1.6 \times 10^{14} \text{ G}$) [28] and should see the highest possible dark matter flux [20]. Axions will encounter a plasma frequency at some radius that equals its mass, and the axion can resonantly convert into a photon at that location [20]. The most promising axion mass range, 1–100 μeV , corresponds to radio frequencies 200 MHz to 20 GHz.

In this *Letter*, we present broad-band radio telescope

observations of PSR J1745–2900. We obtain 95% confidence limits on resonant axion-photon conversion emission line flux density from the magnetar spanning 40% of the 1–38.5 GHz band. We translate these flux limits into limits on $g_{a\gamma\gamma}$ versus m_a based on a hybrid neutron star magnetosphere model and two limiting-case Galactic dark matter profiles. Finally, we discuss model caveats, limitations of the observations, and future observational and theoretical work to expand the $g_{a\gamma\gamma}$ vs. m_a space probed by this technique.

OBSERVATIONS

Interferometric observations of Sgr A* were obtained from the National Science Foundation’s Karl G. Jansky Very Large Array (VLA [29]) data archive. We selected sessions: (1) to maximize on-target integration time, (2) with adequate angular resolution to separate PSR J1745–2900 from Sgr A* (1.7” in both coordinates), (3) to maximize total bandwidth, and (4) to adequately sample the expected emission line bandwidth. VLA A-configuration observations of Sgr A*, 14A-231 and 14A-232, meet these criteria, spanning 40% of the 1–38.5 GHz range (Table I). The gaps in this range are not covered by any extant observations that meet the above criteria.

Each session used the flux density calibrator J1331+3030 (3C286) and the bandpass calibrator J1733–1304. For L- and C-band, the bandpass calibrator was also used for complex gain calibration. The other bands used J1744–3116 for complex gain calibration. Observations of the gain calibrator were interleaved with Sgr A* integrations with 8–30 min cadence. Each band was observed for a full transit of Sgr A*. The correlator was configured to obtain four polarization products (only the two parallel-hand products were used to form Stokes-I spectra below), in 8 to 64 adjacent 64-channel spectral windows with 128 MHz bandwidth each. The

^a The National Radio Astronomy Observatory is a facility of the National Science Foundation operated under cooperative agreement by Associated Universities, Inc.

TABLE I. Very Large Array Summary of Observations.

Band	Frequency (GHz)	Program	Channel Width		Median Velocity (km s ⁻¹)	Integration (s)	Median Beam (arcsec)	PA (°)	MJD ^a	rms ^b (mJy)
			Obs. (MHz)	Smoothed (MHz)						
L	1.008–2.032	14A-231	1	10	2000	10591	2.22 × 1.10 ^c	1	56749	0.33 ^d
C	4.487–6.511	14A-231	2	14	763	10591	0.61 × 0.28	−3	56749	0.099
X	7.987–10.011	14A-231	2	18	600	19148	0.34 × 0.17	−1	56718	0.026 ^e
Ku	12.988–15.012	14A-231	2	20	428	16156	0.24 × 0.11	−1	56726	0.027
Ka	30.476–32.524	14A-232	2	26	247	17053	0.101 × 0.050	−3	56725	0.100
Ka	32.476–34.524	14A-232	2	26	233	17053	0.094 × 0.046	−3	56725	0.116
Ka	34.476–36.524	14A-232	2	28	236	17053	0.089 × 0.045	−4	56725	0.165
Ka	36.476–38.524	14A-232	2	28	224	17053	0.084 × 0.042	−3	56725	0.152

^a Modified Julian Date

^b The rms noise in spectra Gaussian-smoothed to channels of width Δf (Column 5 and Equation 2).

^c The quoted L-band beam is the continuum beam; the synthesized beam in the spectral cube is highly variable due to RFI and the large fractional bandwidth.

^d The rms noise includes residual unmitigated RFI.

^e The rms noise omits the central RFI feature and band edges.

spectral windows were divided into 2 or 4 slightly overlapping baseband groups. The L-band configuration differed: it used spectral windows of 64 MHz bandwidth and 1 MHz channels. All sampling was 8-bit except for the Ka-band session, which used 3-bit sampling. Correlator dump times were 1–5 s.

DATA REDUCTION

All data reduction tasks were performed using CASA [30]. After data flagging, we applied the flux, delay, atmospheric transmission, complex bandpass, and complex gain calibration to the target field. We then performed in-beam phase self-calibration using the Sgr A* continuum, which ranged from 0.5 to 5.6 Jy (L- to Ka-band). We imaged the continuum field and identified the continuum emission of PSR J1745–2900 (20–5 mJy in L to Ka bands) to confirm its coordinate offset from Sgr A*.

We fit a 2D Gaussian to the Sgr A* continuum to set the origin for relative astrometry to locate PSR J1745–2900 based on the bootstrap proper motion solution obtained by [31] that assumes no acceleration or core shift. At the observed angular resolution, Sgr A* is consistent with being a point source. Coordinate offsets from Sgr A* were $(\Delta\alpha, \Delta\delta) = (1.701, -1.679)$ arcsec in all epochs; offsets between epochs differed by no more than 1 mas. The predicted offsets of PSR J1745–2900 from Sgr A* are consistent with the observed continuum position of the magnetar.

We fit and subtracted a linear continuum spectrum from the data in UV (image Fourier) space and formed spectral image cubes using pixels that over-sampled the synthesized beams (which vary across each cube). Sgr A* shows narrow-band spectral structure after the continuum subtraction, some of which are attributable to known molecular lines such as the 14.4881 GHz H₂CO

and 36.795 GHz CH₃CN. Sidelobes from these features are cleaned during cube deconvolution and do not significantly contaminate the magnetar spectrum. The zero-mean magnetar spectra typically reach the theoretical noise.

At the position of the magnetar, we extract a spectrum by summing pixels over the (frequency-dependent) synthesized 2D Gaussian beam. We correct the spectrum for the beam size to capture the total flux density of a point source separately for every channel. In order to assess the significance of features in the magnetar spectrum, which can be highly variable channel-to-channel due to radio frequency interference (RFI) or band edges, we create a noise spectrum by measuring the off-source rms sky noise in each channel. This allows us to create a significance spectrum for each band. We scale the noise spectrum to match the spectral noise measured toward PSR J1745–2900 (this correction is typically a few percent).

The fractional bandwidth predictions for the expected signal range from $\Delta f/f = (v_0/c)^2$ [20], where v_0 is the axion velocity dispersion, to (v_0/c) [21]. We adopt the spinning mirror model whereby the Doppler broadening is dominated by the neutron star rotation [24], producing, on average, $\Delta f/f \simeq \Omega r_c \varepsilon^2/c$, where Ω is the neutron star’s angular frequency, ε is the eccentricity of the elliptical critical surface (which we and [24] set to unity), and r_c is the axion-photon conversion radius. For the latter, we adopt the formulation of [20], assuming polar orientation angle $\theta = \pi/2$ and magnetic offset axis $\theta_m = 0$ (see below, where we marginalize over these unknown angles; as [25] show, ray-tracing is the technically correct approach, and tends to show less variation with

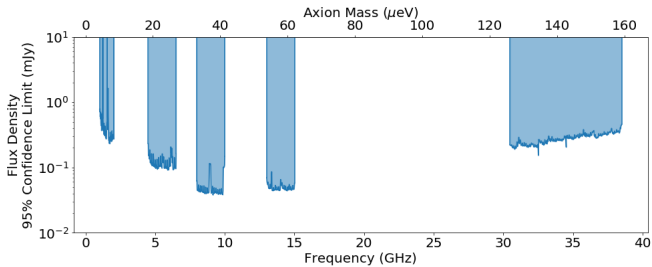


FIG. 1. 95% confidence limits on emission line flux density for channel width $\Delta f = 8.3 \text{ MHz} \times (m_a c^2 / 4.1 \text{ } \mu\text{eV})^{1/3}$.

these angles than the analytic treatment):

$$r_c = 224 \text{ km} \left(\frac{r_0}{10 \text{ km}} \right) \left[\frac{B_0}{10^{14} \text{ G}} \frac{1}{2\pi} \frac{\Omega}{1 \text{ Hz}} \left(\frac{4.1 \text{ } \mu\text{eV}}{m_a c^2} \right)^2 \right]^{1/3} \quad (1)$$

where r_0 is the neutron star radius, B_0 is the magnetic field, and $4.1 \text{ } \mu\text{eV}$ corresponds to an observed frequency of 1 GHz. This leads to an expected line bandwidth:

$$\Delta f = 3.6 \text{ MHz} \left(\frac{\Omega}{1 \text{ Hz}} \right)^{4/3} \left(\frac{m_a c^2}{4.1 \text{ } \mu\text{eV}} \right)^{1/3} \left(\frac{B_0}{10^{14} \text{ G}} \right)^{1/3}. \quad (2)$$

The spin period of PSR J1745–2900 is 3.76 s [32] and the magnetic field is $1.6 \times 10^{14} \text{ G}$ [28]. The expected line width is therefore $\Delta f = 8.3 \text{ MHz} \times (m_a c^2 / 4.1 \text{ } \mu\text{eV})^{1/3}$.

The VLA correlator spectral windows have a strong response dropoff on edge channels and on the edges of the basebands. These channels lack the signal-to-noise for calibration and are flagged, which typically creates single-channel gaps in the spectrum and decreased sensitivity on the spectrum edges. The flagged channels are much narrower than the expected line width. We smooth the magnetar and noise spectra to the expected line width (Equation 2) using a Gaussian kernel [33], and interpolate across missing channels during smoothing (the resulting statistics are not substantially altered by this loss of strict channel-to-channel independence). In L-band there are gaps in the spectrum where RFI-flagged spectral regions are wider than the smoothing kernel.

Table I lists synthesized beam parameters, channel widths, and spectral rms noise values. The Supplemental Material [34] presents the magnetar flux, noise, and

signal-to-noise spectra.

RESULTS

We detect no significant single-channel emission features in the observed bands. The only two channels above 3σ in emission were found in Ka-band (3.1σ and 3.5σ). These departures are consistent with Gaussian noise statistics.

After establishing the lack of significant detections in the observed spectra, we form 95% confidence limits from the sky noise spectra. Figure 1 presents these single-channel confidence limits. These are model-independent limits on the flux density of photons produced by axion conversion in the magnetosphere of PSR J1745–2900 [35]. We present these limits to enable models not treated below to be translated into axion limits.

ANALYSIS

Limits on the axion-photon coupling $g_{a\gamma\gamma}$ obtained from observed flux density limits depend on the magnetar magnetospheric and axion-photon conversion model and on the behavior of the dark matter at the Galactic Center. Our choices — as well as alternatives — are discussed below.

The Magnetar Model

Hook et al. [20] predict the photon flux from axion conversion in a neutron star magnetosphere using a variant of the Goldreich and Julian [36] model. The observed flux density depends on the local dark matter density (ρ_∞) and its velocity dispersion (v_0) and on the neutron star mass, radius, magnetic field, rotation period, distance, viewing angle with respect to the rotation axis, and magnetic misalignment angle from the spin axis (M_{NS} , r_0 , B_0 , P , d , θ , and θ_m , respectively). It also depends on m_a and $g_{a\gamma\gamma}$. Equations 11–13 in [20], modified for the expected bandwidth (Equation 2), yield an expression for the emission line flux density normalized to fiducial values for a nearby pulsar:

$$S_\nu = 1.2 \times 10^{-6} \text{ mJy} \left(\frac{100 \text{ pc}}{d} \right)^2 \left(\frac{m_a}{1 \text{ GHz}} \right)^{4/3} \left(\frac{200 \text{ km s}^{-1}}{v_0} \right) \left(\frac{g_{a\gamma\gamma}}{10^{-12} \text{ GeV}^{-1}} \right)^2 \left(\frac{r_0}{10 \text{ km}} \right) \times \left(\frac{B_0}{10^{14} \text{ G}} \right)^{1/3} \left(\frac{\Omega}{1 \text{ Hz}} \right)^{-8/3} \left(\frac{\rho_\infty}{0.3 \text{ GeV cm}^{-3}} \right) \left(\frac{M_{NS}}{1 M_\odot} \right) \frac{3(\hat{m} \cdot \hat{r})^2 + 1}{|3 \cos \theta \hat{m} \cdot \hat{r} - \cos \theta_m|^{4/3}} \frac{v_c}{c} \quad (3)$$

where $\hat{m} \cdot \hat{r} = \cos \theta_m \cos \theta + \sin \theta_m \sin \theta \cos \Omega t$. The axion

velocity v_c at the conversion point r_c (see Supplement) is

included to correct the conversion probability presented in [20], as discussed in [25]. For a *given* line sensitivity (or observed flux density limit spectrum), one can obtain a track in $g_{a\gamma\gamma}$ versus m_a space above which $g_{a\gamma\gamma}$ is excluded at some confidence level.

For PSR J1745–2900, we assume a radius $r_0 = 10$ km and mass $M_{NS} = 1 M_\odot$. Using the Navarro-Frenk-White

$$g_{a\gamma\gamma} = 3 \times 10^{-11} \text{ GeV}^{-1} \left(\frac{S_\nu}{10 \mu\text{Jy}} \right)^{1/2} \left(\frac{m_a}{1 \text{ GHz}} \right)^{-2/3} \left(\frac{v_0}{200 \text{ km s}^{-1}} \right)^{1/2} \times \left(\frac{\rho_\infty}{6.5 \times 10^4 \text{ GeV cm}^{-3}} \right)^{-1/2} \underbrace{\left(\frac{3(\hat{m} \cdot \hat{r})^2 + 1}{|3 \cos \theta \hat{m} \cdot \hat{r} - \cos \theta_m|^{4/3}} \frac{v_c}{c} \right)^{-1/2}}_{(i)}. \quad (4)$$

The angular term (*i*) in Equation 4 relies on the unknown viewing and magnetic field misalignment angles, so we marginalize over all possible orientations while keeping track of the fraction of the magnetar spin period (if any) that has $r_c < r_0$ (see Supplement). If the conversion radius r_c is less than the neutron star radius, then no conversion occurs and the photon flux vanishes [20]. The analytic value of $r_c < r_0$ is a conservative estimate; ray-tracing suggests that the actual axion-photon conversion can occur over a larger range of angles [25]. Contrary to [20], we find that conversion can still occur up to and beyond 10 GHz. At the low end of the observed Ka-band range, 2.1% of all possible (θ, θ_m) have $r_c < r_0$ at all times; at the high end of the band, this increases to 5.6%. At the high end of the observed Ku band, the fraction of orientations with no emission decreases to 0.16%.

Axion Constraints from Dark Matter Models

Following [20], we use two dark matter models — a generic NFW model and the NFW model plus a central dark matter spike — that roughly bound the weakest and strongest constraints on $g_{a\gamma\gamma}$ given the magnetar model unless the Galactic Center dark matter is cored (see below and Discussion). We use the NFW dark matter model from [38] with $\gamma = 1$, $R_0 = 8.2$ kpc, $r_s = 18.6$ kpc, $v_0 = 300 \text{ km s}^{-1}$, and $\rho_\odot = 0.38 \text{ GeV cm}^{-3}$, which predicts a dark matter density of $6.5 \times 10^4 \text{ GeV cm}^{-3}$ at the 0.1 pc radial distance of the magnetar. The assumed physical distance of PSR J1745–2900 from Sgr A* — itself assumed to reside at the center of the dark matter distribution — is the projected distance (absent an acceleration measurement, one cannot determine the physical distance between Sgr A* and the magnetar [31], but if the magnetar is gravitationally bound to Sgr A*, then the projected separation is likely to be a good approxi-

(NFW [37]) Galactic dark matter profile $\gamma = 1$ model of [38], which has Galactic Center distance $d = 8.2$ kpc (in agreement with the S2 stellar orbital measurement around Sgr A* [39]), scale radius $r_s = 18.6$ kpc, and local dark matter energy density $\rho_\odot = 0.38 \text{ GeV cm}^{-3}$ (see below), one obtains an axion mass-dependent expression for $g_{a\gamma\gamma}$:

mation for the physical separation). For the dark matter spike, we use the above NFW profile modified to include a spike radial index $\gamma_{sp} = 7/3$ and extent $R_{sp} = 0.1$ kpc, which corresponds to a 99.7% upper limit on deviations from a black hole-only orbit of the S2 star about Sgr A* [40]. This model predicts a dark matter density of $6.4 \times 10^8 \text{ GeV cm}^{-3}$ at the magnetar position. All else equal, this dark matter spike model can be considered to be a best-case constraint on $g_{a\gamma\gamma}$. The two models span a factor of 10^4 in dark matter density, which is a factor of 100 in the $g_{a\gamma\gamma}$ constraint. Future studies of the dynamics in the central parsec should improve constraints on the dark matter density encountered by PSR J1745–2900.

Table II lists the median 95% confidence limits on $|g_{a\gamma\gamma}|$ obtained from these end-case dark matter models for each observed band. Figure 2 shows the limits for the two models versus frequency and axion mass. The limits obtained for the standard NFW profile reach $|g_{a\gamma\gamma}| \simeq 6 \times 10^{-12} \text{ GeV}^{-1}$, which is a factor of ~ 40 above the strongest-coupling theoretical model [41]. The limits obtained for the dark matter spike model impinge on the family of theoretical models [41] for m_a in 33.0–41.4 μeV , 53.7–62.1 μeV , and 126.0–159.3 μeV , but do not exclude the canonical KSVZ or DFSZ models [8–11]. If the Galactic dark matter has a flat profile inward of 0.5 kpc (i.e. it is “cored”), then the predicted dark matter density is 12 GeV cm^{-3} at the magnetar, the limits on $g_{a\gamma\gamma}$ are a factor of 100 above the NFW profile limits, and the limits are less constraining than the CAST limits.

DISCUSSION

The limits on $g_{a\gamma\gamma}$ presented here are less stringent than those predicted by [20], even after scaling the telescope sensitivity and integration time. This is due to the expected bandwidth of the conversion emission line; we

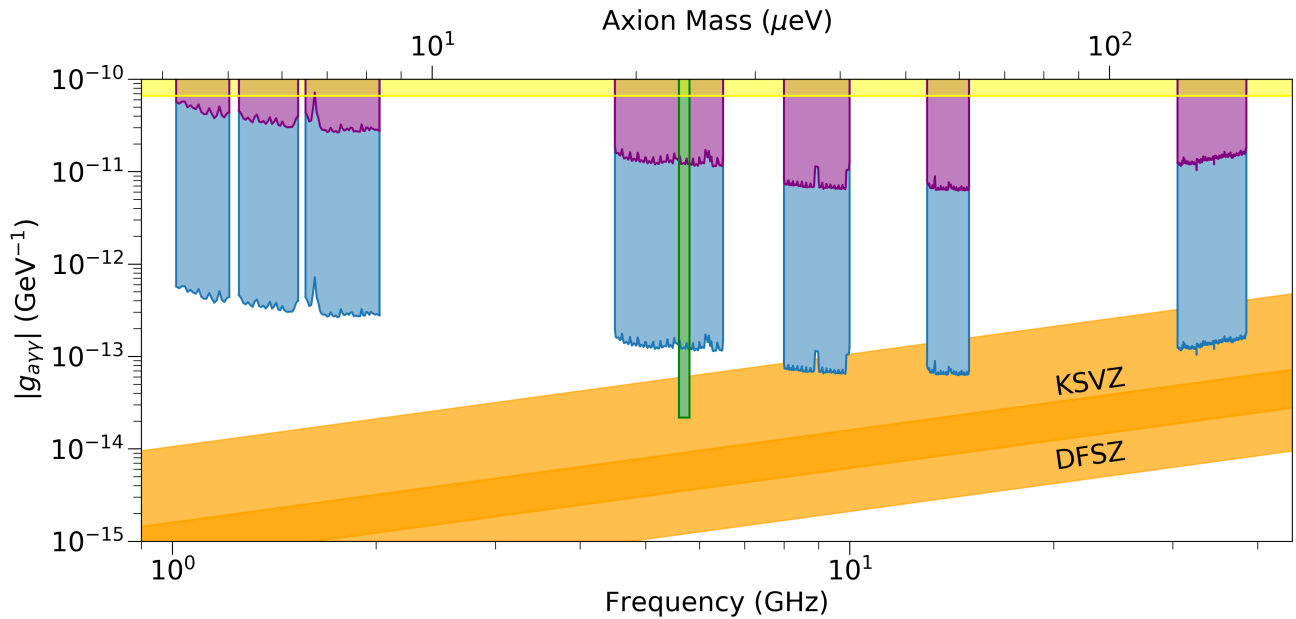


FIG. 2. 95% confidence limits on $g_{a\gamma\gamma}$ for a generic NFW $\gamma = 1$ model with $\rho_{\odot} = 0.38 \text{ GeV cm}^{-3}$ (purple, upper) and the same NFW model plus a central 100 pc dark matter spike (blue, lower). The green bar shows the HAYSTAC limit [18], which has been scaled from a local axion density of 0.45 GeV cm^{-3} to 0.38 GeV cm^{-3} , and the yellow bar shows the CAST 95% confidence limit [42]. Orange loci indicate a range of possible QCD axion models [41], including the canonical KSVZ and DFSZ models [8–11].

TABLE II. Limits on $g_{a\gamma\gamma}$ for two dark matter profile models.

Axion Mass (μeV)	Median $ g_{a\gamma\gamma} $ 95% Confidence Limits	
	NFW Profile (GeV^{-1})	DM Spike (GeV^{-1})
4.2–8.4 ^a	3.4×10^{-11}	3.4×10^{-13}
18.6–26.9	1.3×10^{-11}	1.3×10^{-13}
33.0–41.4	6.9×10^{-12}	7.0×10^{-14}
53.7–62.1	6.5×10^{-12}	6.5×10^{-14}
126.0–159.3	1.4×10^{-11}	1.4×10^{-13}

^a There are gaps in the coverage of this mass range (see Figure 2).

used a line width roughly 10^3 – 10^4 times larger, following the rotating mirror conversion region treatment of [24], which leads to a factor of ~ 300 in $g_{a\gamma\gamma}$. This bandwidth is likely the most conservative choice, and a more physical model for the axion-photon conversion bandwidth will require detailed ray-tracing and a more sophisticated magnetosphere model [25].

The magnetospheres of magnetars must be more complicated than current models assume. Moreover, the resonant conversion of axions into photons will likely be boosted by stimulated emission caused by the ambient photon bath [43]. The expected conversion emission line would be enhanced by the photon occupation number $f_{\gamma} = \pi^2 \rho_{\gamma} / E_{\gamma}^3$, where ρ_{γ} is the specific energy density of stimulating photons (which must match the conver-

sion photons in energy and momentum). Including the contribution from stimulated emission, which is expected to be particularly important in the Galactic Center environment [43], will significantly improve the constraints on $g_{a\gamma\gamma}$ without the need for additional observations. Numerical simulation may be required to correctly characterize the role of stimulated emission in resonant axion-photon conversion in neutron star magnetospheres.

Finally, the constraints on $g_{a\gamma\gamma}$ depend critically on the dark matter energy density in the inner parsec, which remains poorly constrained compared to the other parameters in Equations 3 and 4 (which have uncertainties of order 10–50%). Cuspy versus cored dark matter profiles depend on the dominant baryon physics. Baryons can contract and steepen the central dark matter density, and there is evidence that this has happened in the Galaxy [44], but baryon feedback (e.g. star formation and supernovae) can flatten the central dark matter profile. While a multi-kpc core is disfavored [45], current studies cannot yet probe the inner kpc, so the dark matter density at the magnetar remains an extrapolation. It seems likely, however, that observations of stars and gas combined with dynamical models will soon provide meaningful measurements of the role of dark matter in the Galactic Center. The sensitivity of future telescopic observations will also improve with the advent of large collecting-area facilities such as the Square Kilometer Array, although added sensitivity above a few GHz would require a next-generation

VLA.

CONCLUSIONS

We have demonstrated how radio telescope spectral observations of the magnetar PSR J1745–2900 can produce broad-band limits on axion-photon coupling. This work can be expanded by observing more of the 1–50 GHz spectral window and obtaining longer integration times. Future observations could also increase signal-to-noise by observing in a spectral line pulsar mode, which requires fine time sampling of the neutron star spin period.

The VLA interferometer in its most extended configuration spatially filters out any extended axion conversion spectral line produced in the collective magnetospheres of the as-yet undetected population of Galactic Center neutron stars. An optimal strategy to detect this extended signal would depend on the areal extent of the emission, the magnetized neutron star population, and the dark matter density in the Galactic Center [46].

There are parts of the radio spectrum that will never be observable for axion signals from the ground, such as global positioning bands, large parts of the sub-GHz spectrum due to RFI, the 22 GHz atmospheric water band, and the molecular oxygen band spanning 50–70 GHz. These regions merit special scrutiny by laboratory experiments. Magnetar observations are further limited by the requirement that axions cannot be converted inside the neutron star, above roughly 50 GHz.

We thank the observing, archive, and computing staff at the NRAO who made this work possible. We also thank Konrad Lehnert, Marco Chianese, Andrea Caputo, and Richard Battye for helpful discussions. This research made use of CASA [47], NumPy [48], Matplotlib [49], and Astropy [50], a community-developed core Python package for Astronomy [33, 51].

* jeremy.darling@colorado.edu

- [1] R. D. Peccei and H. R. Quinn, *Phys. Rev. Lett.* **38**, 1440 (1977).
- [2] S. Weinberg, *Phys. Rev. Lett.* **40**, 223 (1978).
- [3] F. Wilczek, *Phys. Rev. Lett.* **40**, 279 (1978).
- [4] J. Preskill, M. B. Wise, and F. Wilczek, *Phys. Lett. B* **120**, 127 (1983).
- [5] M. Dine and W. Fischler, *Physics Letters B* **120**, 137 (1983).
- [6] L. F. Abbott and P. Sikivie, *Physics Letters B* **120**, 133 (1983).
- [7] R. T. Co and K. Harigaya, *arXiv e-prints*, arXiv:1910.02080 (2019), arXiv:1910.02080 [hep-ph].
- [8] J. E. Kim, *Phys. Rev. Lett.* **43**, 103 (1979).
- [9] M. A. Shifman, A. I. Vainshtein, and V. I. Zakharov, *Nuclear Physics B* **166**, 493 (1980).
- [10] M. Dine, W. Fischler, and M. Srednicki, *Physics Letters B* **104**, 199 (1981).
- [11] A. R. Zhitnitskij, *Yadernaya Fizika* **31**, 497 (1980).
- [12] P. Sikivie, *Phys. Rev. Lett.* **51**, 1415 (1983).
- [13] M. Arik and et al. (CAST), *Phys. Rev. Lett.* **112**, 091302 (2014).
- [14] M. Arik and et al. (CAST), *Phys. Rev. D* **92**, 021101 (2015).
- [15] S. J. Asztalos and et al. (ADMX), *Phys. Rev. D* **64**, 092003 (2001).
- [16] S. J. Asztalos and et al., *Phys. Rev. Lett.* **104**, 041301 (2010).
- [17] B. M. Brubaker and et al., *Phys. Rev. Lett.* **118**, 061302 (2017).
- [18] L. Zhong, S. Al Kenany, K. M. Backes, B. M. Brubaker, S. B. Cahn, G. Carosi, Y. V. Gurevich, W. F. Kindel, S. K. Lamoreaux, K. W. Lehnert, S. M. Lewis, M. Malnou, R. H. Maruyama, D. A. Palken, N. M. Rapidis, J. R. Root, M. Simanovskaia, T. M. Shokair, D. H. Speller, I. Urdinaran, and K. A. Van Bibber, *Physical Review D* **97**, 092001 (2018).
- [19] A. Arvanitaki, M. Baryakhtar, and X. Huang, *Phys. Rev. D* **91**, 084011 (2015), arXiv:1411.2263 [hep-ph].
- [20] A. Hook, Y. Kahn, B. Safdi, and Z. Sun, *Phys. Rev. Lett.* **121**, 241102 (2018).
- [21] F. P. Huang, K. Kadota, T. Sekiguchi, and H. Tashiro, *Physical Review D* **97**, 123001 (2018).
- [22] S. Mukherjee, R. Khatri, and B. D. Wandelt, *JCAP* **2018**, 045 (2018), arXiv:1801.09701 [astro-ph.CO].
- [23] F. V. Day and J. I. McDonald, *JCAP* **2019**, 051 (2019), arXiv:1904.08341 [hep-ph].
- [24] R. A. Battye, B. Garbrecht, J. I. McDonald, F. Pace, and S. Srinivasan, *Phys. Rev. D* **102**, 023504 (2020), arXiv:1910.11907 [astro-ph.CO].
- [25] M. Leroy, M. Chianese, T. D. P. Edwards, and C. Weniger, *Phys. Rev. D* **101**, 123003 (2020), arXiv:1912.08815 [hep-ph].
- [26] T. D. P. Edwards, M. Chianese, B. J. Kavanagh, S. M. Nissanke, and C. Weniger, *Phys. Rev. Lett.* **124**, 161101 (2020), arXiv:1905.04686 [hep-ph].
- [27] S. Mukherjee, D. N. Spergel, R. Khatri, and B. D. Wandelt, *JCAP* **2020**, 032 (2020), arXiv:1908.07534 [astro-ph.CO].
- [28] K. Mori and et al., *ApJ* **770**, L23 (2013).
- [29] The National Radio Astronomy Observatory is a facility of the National Science Foundation operated under cooperative agreement by Associated Universities, Inc.
- [30] McMullin, J. P., Waters, B., Schiebel, D., Young, W., & Golap, K. 2007, *Astronomical Data Analysis Software and Systems XVI* (ASP Conf. Ser. 376), ed. R. A. Shaw, F. Hill, & D. J. Bell (San Francisco, CA: ASP), 127. See also <https://science.nrao.edu/facilities/vla/data-processing/pipeline> for the CASA calibration pipeline and <https://science.nrao.edu/facilities/vla/data-processing> for VLA calibration and analysis.
- [31] G. C. Bower, A. Deller, P. Demorest, A. Brunthaler, H. Falcke, M. Moscibrodzka, R. M. O’Leary, R. P. Eatough, M. Kramer, K. J. Lee, L. Spitler, G. Desvignes, A. P. Rushton, S. Doeleman, and M. J. Reid, *The Astrophysical Journal* **798**, 120 (2015).
- [32] J. A. Kennea and et al., *ApJ* **770**, L24 (2013).
- [33] A. M. Price-Whelan, B. M. Sipőcz, H. M. Günther, P. L. Lim, S. M. Crawford, S. Conseil, D. L. Shupe, M. W. Craig, N. Dencheva, A. Ginsburg, J. T. VanderPlas, L. D.

- Bradley, D. Pérez-Suárez, M. de Val-Borro, P. Paper Contributors, T. L. Aldcroft, K. L. Cruz, T. P. Robitaille, E. J. Tollerud, A. Coordination Committee, C. Ardelean, T. Babej, Y. P. Bach, M. Bachetti, A. V. Bakanov, S. P. Bamford, G. Barentsen, P. Barmby, A. Baumbach, K. L. Berry, F. Biscani, M. Boquien, K. A. Bostroem, L. G. Bouma, G. B. Brammer, E. M. Bray, H. Breytenbach, H. Buddelmeijer, D. J. Burke, G. Calderone, J. L. Cano Rodríguez, M. Cara, J. V. M. Cardoso, S. Cheedella, Y. Copin, L. Corrales, D. Crichton, D. D'Avella, C. Deil, É. Depagne, J. P. Dietrich, A. Donath, M. Droettboom, N. Earl, T. Erben, S. Fabbro, L. A. Ferreira, T. Finethy, R. T. Fox, L. H. Garrison, S. L. J. Gibbons, D. A. Goldstein, R. Gommers, J. P. Greco, P. Greenfield, A. M. Groener, F. Grollier, A. Hagen, P. Hirst, D. Homeier, A. J. Horton, G. Hosseinzadeh, L. Hu, J. S. Hunkeler, Ž. Ivezić, A. Jain, T. Jenness, G. Kanarek, S. Kendrew, N. S. Kern, W. E. Kerzendorf, A. Khvalko, J. King, D. Kirkby, A. M. Kulkarni, A. Kumar, A. Lee, D. Lenz, S. P. Littlefair, Z. Ma, D. M. Macleod, M. Mastropietro, C. McCully, S. Montagnac, B. M. Morris, M. Mueller, S. J. Mumford, D. Muna, N. A. Murphy, S. Nelson, G. H. Nguyen, J. P. Ninan, M. Nöthe, S. Ogaz, S. Oh, J. K. Parejko, N. Parley, S. Pascual, R. Patil, A. A. Patil, A. L. Plunkett, J. X. Prochaska, T. Rastogi, V. Reddy Janga, J. Sabater, P. Sakurikar, M. Seifert, L. E. Shertbert, H. Sherwood-Taylor, A. Y. Shih, J. Sick, M. T. Silbiger, S. Singanamalla, L. P. Singer, P. H. Sladen, K. A. Sooley, S. Sornarajah, O. Streicher, P. Teuben, S. W. Thomas, G. R. Tremblay, J. E. H. Turner, V. Terrón, M. H. van Kerkwijk, A. de la Vega, L. L. Watkins, B. A. Weaver, J. B. Whitmore, J. Woillez, V. Zabalza, and A. Contributors, *AJ* **156**, 123 (2018).
- [34] See Supplemental Material at [URL].
- [35] Our assumption about the expected signal bandwidth does depend on models for the magnetar, but is $\mathcal{O}(v_0/c)$.
- [36] P. Goldreich and W. H. Julian, *ApJ* **157**, 869 (1969).
- [37] J. F. Navarro, C. S. Frenk, and S. D. M. White, *ApJ* **462**, 563 (1996), arXiv:astro-ph/9508025 [astro-ph].
- [38] P. J. McMillan, *MNRAS* **465**, 76 (2017), arXiv:1608.00971 [astro-ph.GA].
- [39] R. Abuter, A. Amorim, M. Bauböck, J. P. Berger, H. Bonnet, W. Brandner, Y. Clénet, V. Coudé du Foresto, P. T. de Zeeuw, J. Dexter, G. Duvert, A. Eckart, F. Eisenhauer, N. M. Förster Schreiber, P. Garcia, F. Gao, E. Gendron, R. Genzel, O. Gerhard, S. Gillessen, M. Habibi, X. Haubois, T. Henning, S. Hippler, M. Horrobin, A. Jiménez-Rosales, L. Jocou, P. Kervella, S. Lacour, V. Lapeyrère, J.-B. Le Bouquin, P. Léna, T. Ott, T. Paumard, K. Perraut, G. Perrin, O. Pfuhl, S. Rabien, G. Rodríguez Coira, G. Rousset, S. Scheithauer, A. Sternberg, O. Straub, C. Straubmeier, E. Sturm, L. J. Tacconi, F. Vincent, S. von Fellenberg, I. Waisberg, F. Widmann, E. Wieprecht, E. Wiezorrek, J. Woillez, and S. Yazici, *Astronomy & Astrophysics* **625**, L10 (2019).
- [40] T. Lacroix, *Astronomy and Astrophysics* **619**, 46 (2018), arXiv:1801.01308.
- [41] L. Di Luzio, F. Mescia, and E. Nardi, *Physical Review Letters* **118** (2017), 10.1103/PhysRevLett.118.031801, arXiv:1610.07593.
- [42] V. Anastassopoulos, S. Aune, K. Barth, A. Belov, H. Bräuninger, G. Cantatore, J. M. Carmona, J. F. Castel, S. A. Cetin, F. Christensen, J. I. Collar, T. Dafni, M. Davenport, T. A. Decker, A. Dermenev, K. Desch, C. Eleftheriadis, G. Fanourakis, E. Ferrer-Ribas, H. Fischer, J. A. García, A. Gardikiotis, J. G. Garza, E. N. Gazis, T. Gerasis, I. Giomataris, S. Gninenko, C. J. Hailey, M. D. Hasinoff, D. H. Hoffmann, F. J. Iguaz, I. G. Irastorza, A. Jakobsen, J. Jacoby, K. Jakovcic, J. Kaminski, M. Karuza, N. Kralj, M. Kremar, S. Kostoglou, C. Krieger, B. Lakic, J. M. Laurent, A. Liolios, A. Ljubicic, G. Luzón, M. Maroudas, L. Miceli, S. Neff, I. Ortega, T. Papaevangelou, K. Paraschou, M. J. Pivovarov, G. Raffelt, M. Rosu, J. Ruz, E. R. Chóliz, I. Savvidis, S. Schmidt, Y. K. Semertzidis, S. K. Solanki, L. Stewart, T. Vafeiadis, J. K. Vogel, S. C. Yildiz, and K. Zioutas, *Nature Physics* **13**, 584 (2017), arXiv:1705.02290.
- [43] A. Caputo, M. Regis, M. Taoso, and S. J. Witte, *Journal of Cosmology and Astroparticle Physics* **2019** (2019), 10.1088/1475-7516/2019/03/027, arXiv:1811.08436.
- [44] M. Cautun, A. Benítez-Llambay, A. J. Deason, C. S. Frenk, A. Fattahi, F. A. Gómez, R. J. J. Grand, K. A. Oman, J. F. Navarro, and C. M. Simpson, *MNRAS* **494**, 4291 (2020), arXiv:1911.04557 [astro-ph.GA].
- [45] D. Hooper, *Physics of the Dark Universe* **15**, 53 (2017), arXiv:1608.00003.
- [46] B. R. Safdi, Z. Sun, and A. Y. Chen, *Physical Review D* **99** (2019), 10.1103/PhysRevD.99.123021, arXiv:1811.01020.
- [47] J. P. McMullin, B. Waters, D. Schiebel, W. Young, and K. Golap, in *Astronomical Data Analysis Software and Systems XVI*, *Astronomical Society of the Pacific Conference Series*, Vol. 376, edited by R. A. Shaw, F. Hill, and D. J. Bell (2007) p. 127.
- [48] S. van der Walt, S. C. Colbert, and G. Varoquaux, *Computing in Science Engineering* **13**, 22 (2011).
- [49] J. D. Hunter, *Computing in Science Engineering* **9**, 90 (2007).
- [50] [Http://www.astropy.org](http://www.astropy.org).
- [51] Astropy Collaboration, T. P. Robitaille, E. J. Tollerud, P. Greenfield, M. Droettboom, E. Bray, T. Aldcroft, M. Davis, A. Ginsburg, A. M. Price-Whelan, W. E. Kerzendorf, A. Conley, N. Crighton, K. Barbary, D. Muna, H. Ferguson, F. Grollier, M. M. Parikh, P. H. Nair, H. M. Unther, C. Deil, J. Woillez, S. Conseil, R. Kramer, J. E. H. Turner, L. Singer, R. Fox, B. A. Weaver, V. Zabalza, Z. I. Edwards, K. Azalee Bostroem, D. J. Burke, A. R. Casey, S. M. Crawford, N. Dencheva, J. Ely, T. Jenness, K. Labrie, P. L. Lim, F. Pierfederici, A. Pontzen, A. Ptak, B. Refsdal, M. Servillat, and O. Streicher, *A&A* **558**, A33 (2013), arXiv:1307.6212 [astro-ph.IM].
- [52] A. Hook, Y. Kahn, B. R. Safdi, and Z. Sun, *Physical Review Letters* **121** (2018), 10.1103/PhysRevLett.121.241102, arXiv:1804.03145.

A Search for Axionic Dark Matter Using the Magnetar PSR J1745–2900
Supplementary Material

Jeremy Darling

This Supplementary Material presents the radio spectra, noise spectra, and significance spectra of the individual bands used to derive limits on the axion-photon coupling $g_{a\gamma\gamma}$ versus axion mass m_a presented in the main Letter. We also present a discussion of the impact of the magnetar’s rotation and magnetic field axes on the translation of flux density limits into limits on $g_{a\gamma\gamma}$.

SPECTRA OF THE MAGNETAR PSR J1745–2900

Figures 1–5 show the continuum-subtracted flux density spectra, noise spectra, and significance spectra used for flux density and $g_{a\gamma\gamma}$ limits.

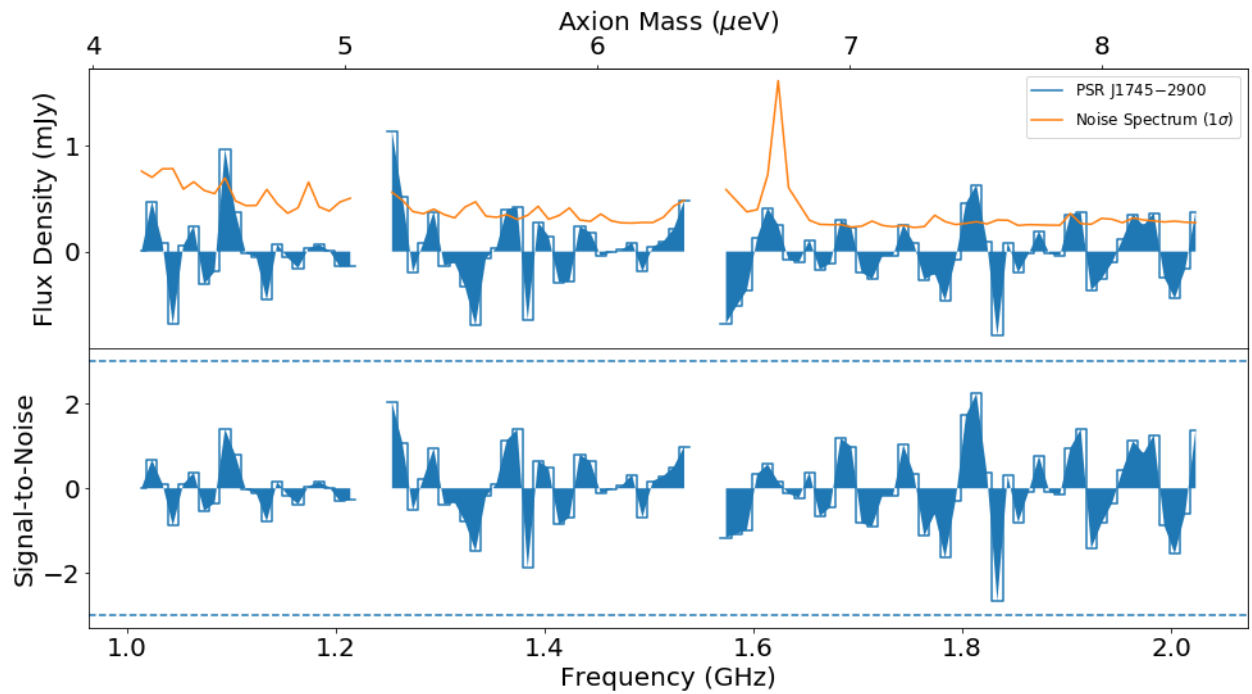


FIG. 1. L-band flux density, noise, and signal-to-noise spectra. The upper spectrum provides limits on $g_{a\gamma\gamma}$, while the lower spectrum indicates the significance of spectral features.

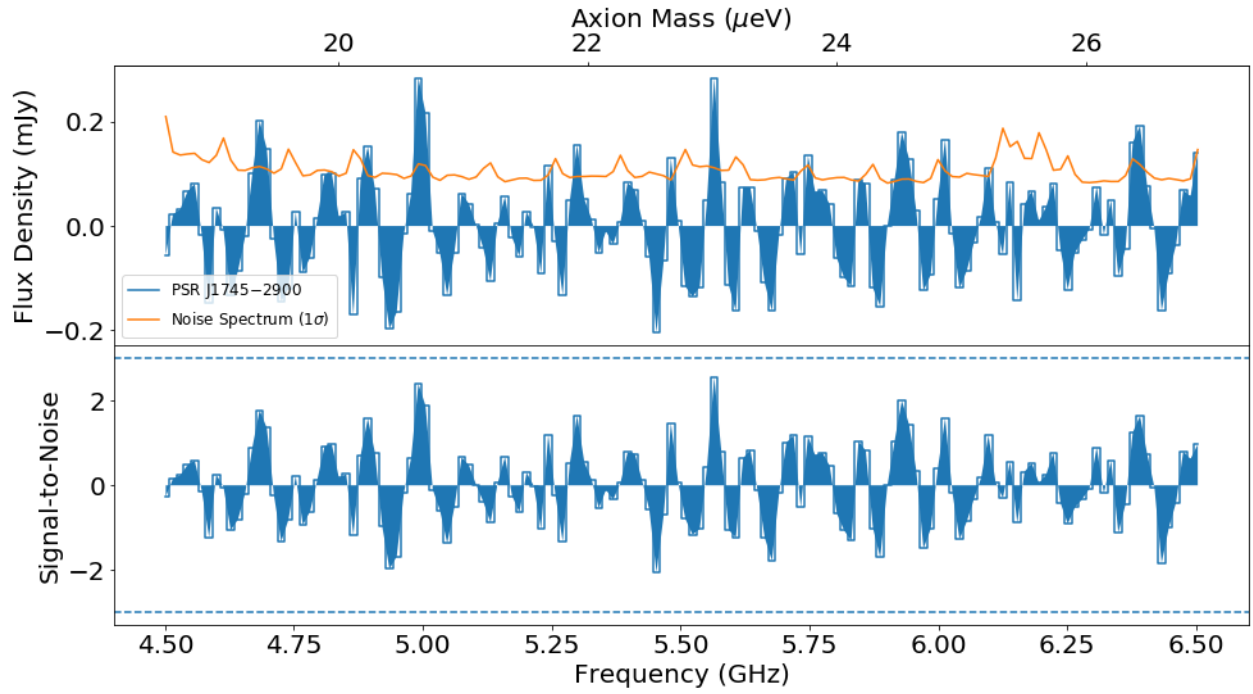


FIG. 2. C-band flux density, noise, and signal-to-noise spectra.

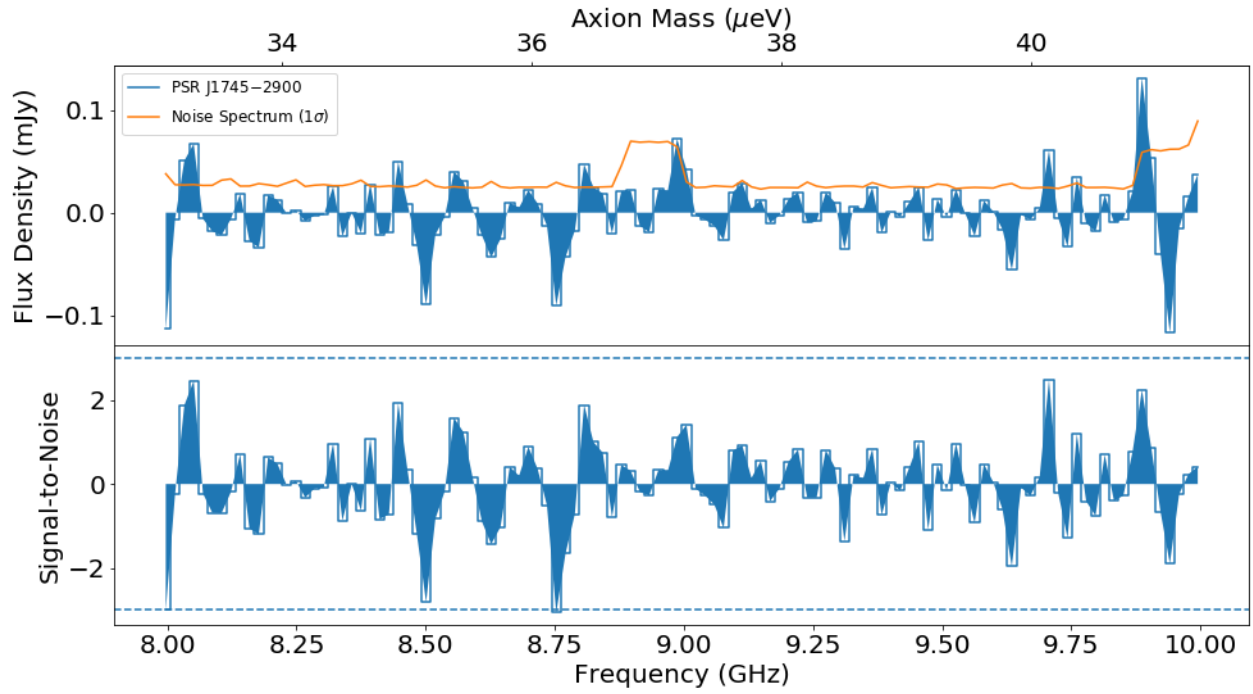


FIG. 3. X-band flux density, noise, and signal-to-noise spectra.

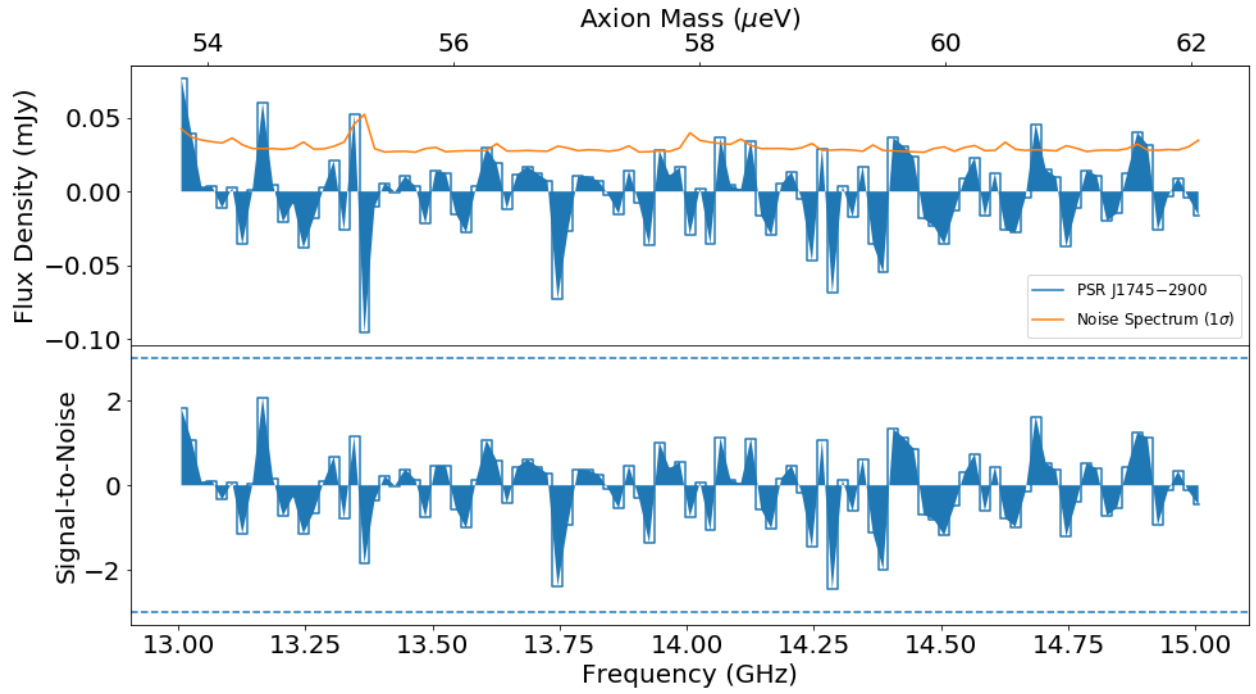


FIG. 4. Ku-band flux density, noise, and signal-to-noise spectra.

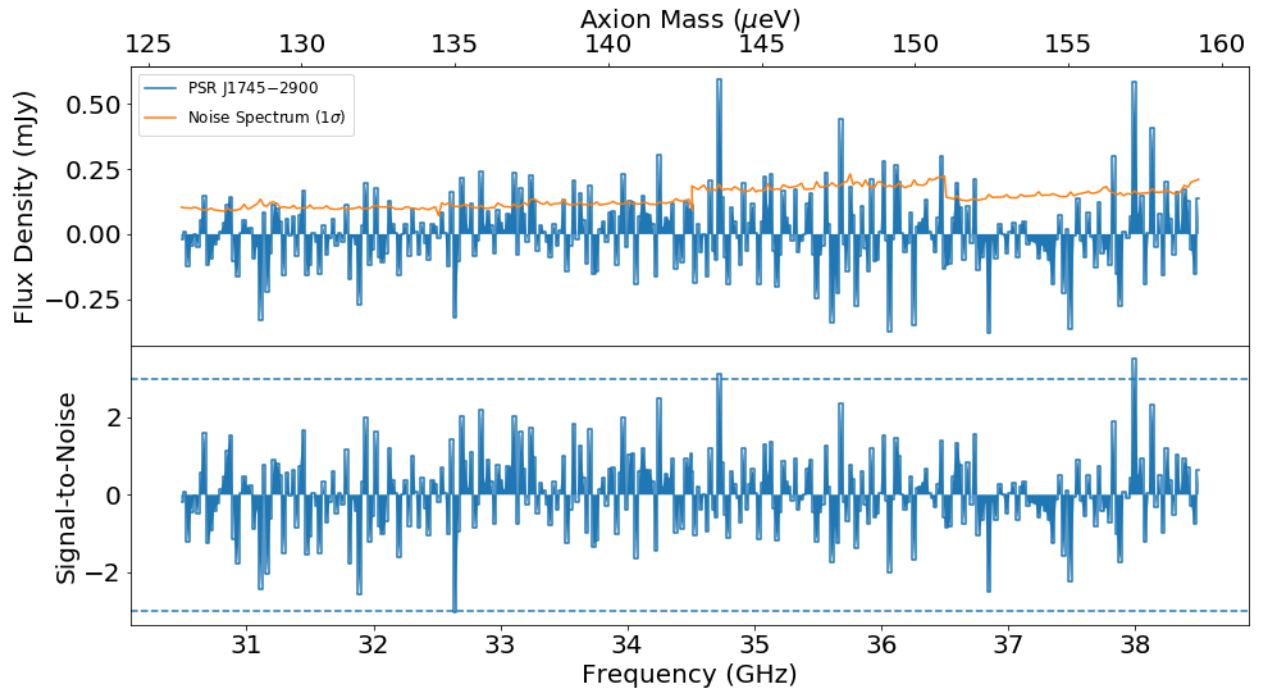


FIG. 5. Ka-band flux density, noise, and signal-to-noise spectra. The four overlapping basebands listed in Table I of the main Letter were combined into a single spectrum.

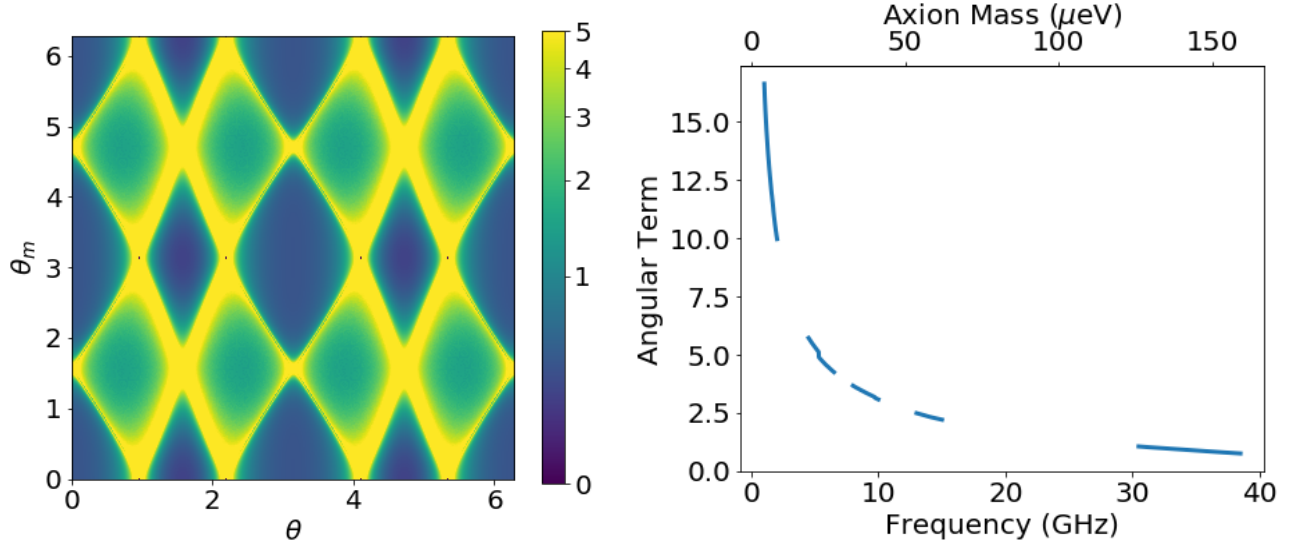


FIG. 6. Left: Time-averaged angular term at 10 GHz plotted for the unknown viewing (θ) and magnetic dipole orientation (θ_m) angles of the magnetar. Right: Angle-marginalized and time-averaged angular term (i) versus frequency.

IMPACT OF THE MAGNETAR SPIN AND MAGNETIC FIELD AXES ON AXION LIMITS

The angular term (i) in Equation 4 of the main Letter modulates the signal, and the modulation time is less than the integration time of the observations, so we average the expected signal over the period of the magnetar for each frequency channel. Moreover, the unknown magnetar spin axis orientation angle θ and magnetic dipole offset angle θ_m impact both the emitted flux density (main Letter, Equation 3) and the axion-photon conversion radius r_c [52]:

$$r_c = 224 \text{ km} \left(\frac{r_0}{10 \text{ km}} \right) \left[\frac{B_0}{10^{14} \text{ G}} \frac{1}{2\pi} \frac{\Omega}{1 \text{ Hz}} \left(\frac{4.1 \mu\text{eV}}{m_a c^2} \right)^2 \right]^{1/3} |3 \cos \theta \hat{m} \cdot \hat{r} - \cos \theta_m|^{1/3}. \quad (1)$$

When $r_c < r_0$ no axion conversion occurs, so the rotation period-averaged flux density will be “censored” in a frequency-dependent manner. The velocity at the conversion point is $v_c^2 \simeq 2GM_{NS}/r_c$ [24].

For each observed frequency channel and possible (θ, θ_m) pair, we create an emission profile over the period of the magnetar rotation that includes no emission when $r_c < r_0$. We calculate a time-integrated flux density, and we marginalize these flux densities at each channel over all (θ, θ_m) . Figure 6 shows an example at 10 GHz of the influence of θ and θ_m on the angular term (i) that includes time-averaging including times when $r_c < r_0$. We also plot the net result of the marginalization over these unknown angles versus frequency and equivalent axion mass. These time-averaged and angle-marginalized angular terms are used in the calculation to place limits on $g_{a\gamma\gamma}$ (main Letter, Equation 4).